

# The effect of an attenuated continuum on the coronal line spectrum of NGC 1068 and the Circinus galaxy.

L.S.Nazarova<sup>1,2</sup>, P.T.O'Brien<sup>1</sup>, M.J.Ward<sup>1</sup>

<sup>1</sup> Department of Physics & Astronomy, University of Leicester, University Road, Leicester, LE1 7RH, U.K.

<sup>2</sup> Astronomical Society, Sternberg Astronomical Institute, Universitetskij prosp.13, Moscow, 119899, Russia

Received/ Accepted

**Abstract.** We present photoionization models of the optical and IR coronal line spectrum in NGC 1068 and the Circinus galaxy. The line fluxes have been calculated using (a) a non-thermal (nuclear) continuum source and (b) the non-thermal continuum plus a UV bump due to a stellar cluster. We take into account the effect of attenuation of these continua by gas with column density  $10^{22}$  cm<sup>-2</sup> located between the nucleus and the coronal line region. The calculated coronal line ratios are in a good agreement with those observed in NGC 1068 for a model in which about 40% of the line emission comes from gas illuminated by unattenuated, non-thermal continuum, and about 60% from gas illuminated by attenuated, non-thermal continuum. The electron density of the coronal line emitting gas in NGC 1068 is found to be  $10^4$  cm<sup>-3</sup>. In the Circinus galaxy the coronal line emission comes from gas with electron density  $10^3$  cm<sup>-3</sup> illuminated entirely by attenuated, non-thermal continuum. The derived ionization parameters for both coronal line regions are very similar, but the different densities imply a higher ionizing photon flux in NGC 1068, consistent with the higher observed excitation state of the line emitting gas in that galaxy. A possible geometry of the coronal line region of both galaxies is discussed, in which the distribution of the attenuating gas may be strongly affected by the relative strength of the nuclear radio-jet. The stronger radio-jet in NGC 1068 may have cleared a channel through the NLR allowing some unattenuated nuclear continuum to illuminate part of the coronal line region.

**Key words:** galaxies:active – galaxies: nuclei – galaxies: individual (NGC 1068, Circinus) – galaxies: Seyfert – modelling: coronal region

## 1. Introduction

Coronal lines correspond to high-excitation, forbidden transitions of ionized species with ionization potentials,  $E \geq 100$  eV. The study of the optical coronal lines —

the so-called iron coronal lines [Fe VII] $\lambda$ 6087, [Fe X] $\lambda$ 6375, [Fe XI] $\lambda$ 7892 and [Fe XIV] $\lambda$ 5303 — has a long history beginning with the original work of Seyfert (1943). Recently interest in the subject has revived following the detection of near-IR coronal lines (Oliva & Moorwood 1990; Oliva et al. 1994). Infrared observations of NGC 1068 and the Circinus galaxy show the presence of strong coronal line emission, such as [Si VI] $\lambda$ 1.963( $\mu$ m), [Si VII] $\lambda$ 2.483( $\mu$ m), [S VIII] $\lambda$ 9912, [S IX] $\lambda$ 1.25235( $\mu$ m), [Si IX] $\lambda$ 3.934( $\mu$ m) and [Si X] $\lambda$ 1.4305( $\mu$ m), (Oliva et al. 1994; Marconi et al. 1996; Moorwood et al. 1996; Thompson 1996; Oliva 1997). The energy needed to produce these ions is in the range 167–351 eV. The optical iron coronal lines have ionization potentials of 100–361 eV. Thus, modelling of these coronal lines can provide important information concerning the shape of the EUV ionizing continuum in the energy range 100–360 eV.

Investigation of the origin of the iron coronal lines show that they are not fitted well by models which assume gas either purely collisionally ionized by fast shocks or photoionized by hot stars (Viegas-Aldrovandi & Contini 1989; Oliva et al. 1994; Marconi et al. 1996). For example, the observed [Si VI]/[Fe VII] ratio in NGC 1068 is better predicted by photoionization models (Marconi et al. 1996). Although Marconi et al. did not exclude some contribution to the coronal line emission in NGC 1068 from shocks or X-rays emitted by a shock front, they suggested that the coronal line region is predominantly photoionized. Recent long-slit, HST observations of NGC 1068 obtained by Axon et al. (1998) (closest spectrum to the proposed nucleus is at  $\sim 1.5''$ ) have shown that some of the strong [Fe VII] $\lambda$ 3769 emission coincides with the radio-jet axis. In the Circinus galaxy shock heating is effectively excluded because the coronal line widths are less than  $100$  km s<sup>-1</sup>.

The most likely source of excitation of the coronal lines is photoionization by the hard UV continuum from a “bare” Seyfert nucleus (Korista & Ferland 1989; Oliva et al. 1994; Marconi et al. 1996; Ferguson et al. 1997). Ferguson et al. found that the coronal line gas is likely to be dust free and that the ionization parameter,  $U$ , and the gas electron-density,  $N_e$ , and temperature,  $T_e$ , in the coronal

line region are  $-2.0 \leq \text{Log } U \leq 0.75$ ,  $10^2 \leq N_e \leq 10^{8.5} \text{ cm}^{-3}$  and  $12\,000 \leq T_e \leq 150\,000 \text{ K}$  respectively.

In addition to the range of physical parameters investigated by Ferguson et al. (1997) one more — the shape of the ionizing continuum — should be considered. Indeed, it is difficult to model successfully the coronal line ratios even in the two best studied galaxies, NGC 1068 and Circinus, by assuming just different physical conditions in the line emitting gas. For example, the observed  $[\text{Fe VII}]/[\text{Fe X}]$  ratio is  $6.3 \pm 0.9$  in NGC 1068 and  $0.47 \pm 0.08$  in Circinus. The  $[\text{Si IX}]/[\text{Si VI}]$  ratio is  $0.63 \pm 0.10$  in NGC 1068 and  $2.12 \pm 0.32$  in Circinus (Marconi et al. 1996). It is difficult to explain such striking differences in these ratios based on photoionization models of a coronal line region with solar abundances ionized by a continuum similar to that of a typical Seyfert galaxy (Ferguson et al. 1997).

In this paper we examine the effect of four different continuum shapes on the coronal line intensities predicted by photoionization models for NGC 1068 and the Circinus galaxy. The nuclear continuum, henceforth referred to as the ‘non-thermal continuum’ to distinguish it from any stellar contribution (discussed below), arises from the unresolved, nuclear region around the central black hole. This nuclear continuum may itself be partly thermal emission from an accretion disk. We also consider the possible effect of a strong ‘UV bump’, which could be an additional ionization source for low-ionization coronal species, such as  $[\text{Fe VII}]$  and  $[\text{Si VI}]$ , compared to high-ionization species, like  $[\text{Fe X}]$  and  $[\text{Si IX}]$ . The most likely explanation for a UV bump in NGC 1068 is the presence of a young stellar cluster near to the nucleus (Thatte et al. 1998). Nazarova (1995) found that the strong  $[\text{Ne V}]\lambda 3425$  emission from the ENLR in NGC 1068 could be explained if the shape of the ionizing continuum is the sum of both non-thermal and thermal components. The Circinus galaxy is also characterized by circumnuclear starburst activity. Star formation activity has been traced by  $\text{H}\alpha$  (Marconi et al. 1994), and the Br recombination line emission peaks at radius  $\approx 200 \text{ pc}$  (Moorwood & Oliva 1994).

As the ionization potentials for the coronal lines are located in the energy range which can be significantly affected by even a relatively modest amount of continuum attenuation (see Fig. 2), we also examine the effect of attenuation of the nuclear and nuclear+stellar continua by gas located between the nucleus and the coronal line region. Photoionization models for the ENLR in NGC 1068 show that the ENLR may be illuminated by an attenuated continuum (Evans & Dopita, 1986; Bergeron et al. 1989; Binette et al. 1996; Nazarova et al. 1998).

The paper is organized as follows: the adopted parameters of the models are discussed in section 2; the modelled surface-luminosity of the coronal line regions of NGC 1068 and the Circinus galaxy for different lines and for the four different continuum shapes are presented in section 3 and the discussion and conclusions are given in sections 4 and 5 respectively.

## 2. The model parameters

### 2.1. Luminosity of the central source

The observed, electron-scattered nuclear-flux of NGC 1068 in the spectral range between  $10^{14.6}$  and  $10^{18.4} \text{ Hz}$  is  $1.5 \times 10^{-10} \text{ erg cm}^{-2} \text{ s}^{-1}$  (Pier et al. 1994). The corresponding luminosity of  $3.5 \times 10^{42} \text{ erg s}^{-1}$ , adopting a distance of 14.4 Mpc ( $1'' = 72 \text{ pc}$ ; Tully 1988), provides a lower limit to the intrinsic nuclear luminosity. In our previous paper on NGC 1068 (Nazarova et al. 1998), we found that the observed high-excitation ENLR could be successfully modelled if the intrinsic nuclear luminosity is actually  $3.6 \times 10^{44} \text{ erg s}^{-1}$  between  $10^{14.6}$  and  $10^{18.4} \text{ Hz}$ . We adopt the same luminosity, which is approximately half the FIR luminosity of NGC 1068 found by Telesco and Harper (1980). This intrinsic luminosity implies a scattering efficiency of 1%, consistent with that estimated by Pier et al. (1994).

The bolometric FIR luminosity of the Circinus galaxy is  $\approx 4 \times 10^{43} \text{ erg s}^{-1}$  (Moorwood & Glass 1984; Ghosh et al. 1992), adopting a distance of 4 Mpc ( $1'' = 20 \text{ pc}$ ). The observed X-ray luminosity of the hidden nucleus of the Circinus galaxy is  $\approx 4 \times 10^{41} \Omega/2\pi$ , where  $\Omega$  is the solid angle subtended at the nucleus by the visible part of the reflecting matter (Matt et al. 1996). Moorwood and Glass (1984) and Forbes and Norris (1998) suggest that the FIR luminosity in Circinus may be dominated by processes associated with circumnuclear star formation. In contrast, Moorwood et al. (1996) suggest the starburst contributes about 10%. Given the uncertainties in the continuum shape, dust covering factor and in the isotropy of the ionizing continuum we derive an ionizing luminosity in an analogous way to that used for NGC 1068. We assume that the FIR luminosity of the Circinus galaxy is an upper limit to the ionizing luminosity, and that approximately half of it could be due to dust heated by stars. Thus, we adopt an ionizing luminosity for the Circinus galaxy of  $2 \times 10^{43} \text{ erg s}^{-1}$ . An increase or decrease in this number by (say) 50% would make no significant difference to the conclusions reached in this paper.

### 2.2. Location and kinematics of the coronal line region

#### 2.2.1. NGC 1068

The observed coronal line emission in NGC 1068 peaks  $\approx 0.5''$  NE of the nucleus and extends over  $\approx 4''$  (Marconi et al. 1996). This position is close to that found by Marconi et al. for other similar ionization-potential lines at widely different wavelengths, such as  $[\text{S III}]\lambda 9069$  and  $\text{He II}\lambda 4686$  and  $[\text{Fe XI}]$  and  $[\text{Si IX}]$ . They also found that low-excitation lines with a ionization potential  $E \leq 20 \text{ eV}$  have a mean central velocity of  $\approx 1080 \text{ km s}^{-1}$ , which is close to the systematic velocity, medium excitation lines with  $20 \leq E \leq 100 \text{ eV}$  have a central velocity  $\approx 930 \text{ km s}^{-1}$  and coronal lines with  $E \geq 100 \text{ eV}$  have a central

velocity  $\simeq 850 \text{ km s}^{-1}$ . Although this trend suggests decelerating, outflowing gas, the [Fe XI] and [Si IX] lines in NGC 1068 are significantly narrower than [Fe VII]. One possible reason is that [Fe VII] may have a similar rotational component of velocity as [O III] at the same distance from the central source. Indeed the blue-shifted component of [O III] may be mainly emitted by outflowing material, as it has a velocity-shift similar to the coronal lines, whereas the velocity of the narrow [O III] component is closer to the systematic velocity and is possibly due to rotating material (Alloin 1983). We assume that the coronal line region in NGC 1068 is located between  $0.5''$  and  $4''$  (36–288 pc). Adopting the continuum shapes discussed in Section 2.3, the unattenuated, incidental, monochromatic continuum flux from the central source at the inner radius of the coronal line region is  $\nu F\nu = 10^{2.46} \text{ erg s}^{-1} \text{ cm}^{-2}$  at 0.1 Ryd.

### 2.2.2. The Circinus galaxy

The nucleus of the Circinus galaxy shows a one-sided ionization cone (Marconi et al. 1994) and bipolar, polarized radio lobes (Elmouttie et al. 1995). The size of the coronal region emitting the highest excitation lines, estimated from the [Fe X] image, is  $\approx 10 \text{ pc}$  ( $\approx 0.5''$ ) (Oliva et al. 1994). Other coronal lines are also highly concentrated towards the nucleus. The visible and IR coronal lines are blue-shifted by about  $35 \text{ km s}^{-1}$  in Circinus (Oliva et al.). As the luminosity of the Circinus galaxy is  $\approx 18$  times lower than NGC 1068 and the adopted inner-radius of the coronal line region in NGC 1068 is 36 pc, we adopt an inner radius for the coronal line region in the Circinus galaxy of 8.6 pc. This convenient definition means that the unattenuated, incidental, monochromatic continuum flux from the central source at the inner radius of the coronal line region in the Circinus galaxy is the same as in NGC 1068 (i.e.,  $\nu F\nu = 10^{2.46} \text{ erg s}^{-1} \text{ cm}^{-2}$  at 0.1 Ryd, for the continuum shapes discussed below).

### 2.3. The shape of the ionizing continuum

We model the coronal line intensities of NGC 1068 and the Circinus galaxy using four different ionizing continua. The first is the ‘non-thermal’, nuclear continuum. It should be noted that we refer to this continuum as the non-thermal continuum, although it may in fact have a thermal contribution, simply in order to distinguish it from the continuum discussed below which includes a hot, possibly stellar, UV bump component. The shape of the non-thermal continuum for NGC 1068 was derived from two sources. The UV and X-ray continua were taken from Pier et al. (1994), extrapolated to the EUV region. The rest of the continuum shape was taken as that of the canonical AGN continuum of Mathews & Ferland (1987). This continuum is the same as that used in our previous paper modelling the ENLR in NGC 1068 (Nazarova et al. 1998). The

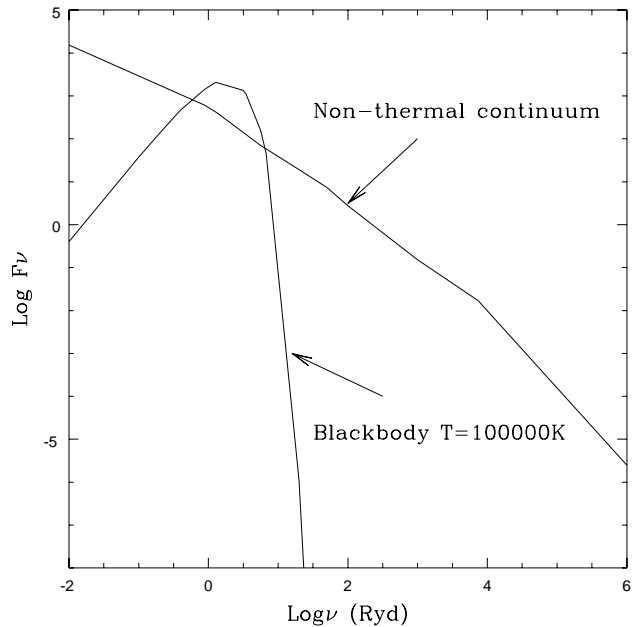


**Fig. 1.** The non-thermal and stellar ( $T=100\,000\text{K}$ ) continua. Both continua are plotted in units of photons  $\text{Ryd}^{-1} \text{ cm}^{-2} \text{ s}^{-1}$  with an arbitrary normalization.

shape of the central continuum for the Circinus galaxy is less well known. The X-ray radiation in the 2–10 keV band is heavily obscured (Matt et al. 1996) and a compact radio synchrotron source is observed in the nucleus (Forbes & Norris 1998). Because of the uncertainties in the shape of the ionizing continuum in the Circinus galaxy we adopt the same continuum shape as for NGC 1068 when modelling the coronal line intensities. The photoionization model with this incident continuum shape is called Model NT.

Based on integral-field spectroscopy, Thatte et al. (1998) suggest that about 10% of the bolometric luminosity in the central  $1''$  of NGC 1068 comes from a moderately-reddened stellar cluster, age 5–13  $\times 10^8$  years, intrinsic size  $\approx 50 \text{ pc}$  surrounding the nucleus. However, they note that the stellar cluster could contribute as much as 50% of the nuclear bolometric luminosity if the cluster age is  $\leq 10^7$  years. An old starburst population is probably present in the Circinus galaxy, located within the innermost 4 pc (Oliva et al. 1994). Moorwood et al. (1996) modelled the IR coronal lines with a central ionizing continuum which has a UV bump peaking around 70 eV. The ASCA data for Circinus are consistent with soft X-ray emission from a circumnuclear starburst (Matt et al. 1996).

Although we are certain of neither the existence nor origin of a UV bump in either NGC 1068 or Circinus, we calculated the coronal line intensities including a ‘UV bump’ component in the incident continuum in addition to the non-thermal continuum. We assume that the UV

bump component can be represented by a blackbody continuum with temperature  $T = 100\,000$  K, a temperature typical of that of the hottest stars (the so-called ‘warmers’, Terlevich & Melnick 1985). The photoionization model with this combined non-thermal + ‘stellar’ continuum is called Model NTS. The non-thermal and stellar continuum components are shown in Fig. 1. The relative contributions to the ionizing flux, as seen by the coronal line gas, due to the non-thermal and stellar components in Model NTS are 33% and 67% respectively. It is difficult to estimate the actual ionizing flux due to the star cluster as seen by the coronal line gas as we cannot be certain of either the distance from the stars to the gas or the stellar luminosity. Here we have deliberately set the stellar ionizing flux seen by the coronal line gas at a high value to examine the effect of such a component.

To construct the other two continua we included the effect of attenuation of both the NT and NTS continua. We used the Cloudy photoionization code (version 90.03; Ferland 1996; Ferland et al. 1998) to calculate the sum of both the transmitted and diffuse continua for an attenuating gas column of  $10^{22}$  cm $^{-2}$  with  $N_e = 10^4$  cm $^{-3}$ , located between the nucleus and the coronal line region. The photoionization models with these attenuated continua are called Models NTA and NTSA respectively. The shapes of the four continua used to model the coronal line regions in NGC 1068 and the Circinus galaxy are shown in Fig. 2.

Adopting these four continuum shapes, all the models were normalized to have the same monochromatic flux illuminating the inner-radius of the coronal line region at 0.1 Ryd as in model NT, namely  $\nu F\nu = 10^{2.46}$  erg s $^{-1}$  cm $^{-2}$ .

### 3. Photoionization models

We calculated the emission line intensities using the CLOUDY photoionization code (version 90.03; Ferland 1996; Ferland et al. 1998) for a slab of gas with solar abundances. Based on the observations, the inner and outer radii of the coronal line region in NGC 1068 were taken to be 36 pc (0.5'') and 288 pc (4'') respectively. The size of the coronal line region in NGC 1068 agrees well with the slit width (4.4'') of the IR spectra (Marconi et al. 1996). For the optical data, we used the dereddened line fluxes in the range 3400–5100Å and 4800–9300Å given by Marconi et al., which were taken with slit widths of 1.4'' and 1.5'' respectively.

The size of the region emitting the high excitation lines in the Circinus galaxy, estimated from the [Fe XI] image, is about 10 pc ( $\approx 0.5''$ ) and the long-slit spectra show that the elongation of the coronal line region is less than 2'' (Oliva et al., 1994). For the Circinus galaxy we took the inner-radius of the coronal line region as 8.6 pc (0.43'') and the outer radius as 68.8 pc (3.44'') (section 2.2.2).

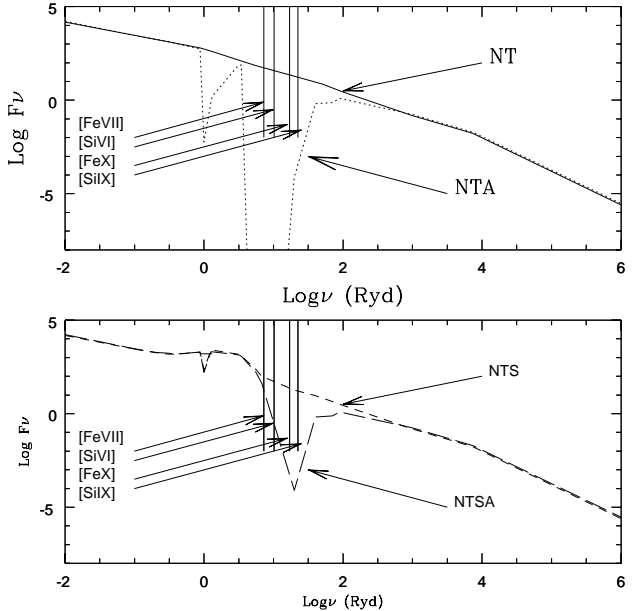


**Fig. 2.** The continua for the four models plotted in units of photons Ryd $^{-1}$  cm $^{-2}$  s $^{-1}$  with arbitrary normalization. The photon energies needed to produce several prominent coronal line species are also indicated.

The coronal line regions in NGC 1068 and the Circinus galaxy are sufficiently large that we normalize all models to the ionization parameter  $U$  at the inner-edge of the coronal line region. The ‘local value’ of  $U$  will of course vary across the region. The line intensities used in this paper were computed by integrating across the entire coronal-line region. The ionization parameter,  $U$ , depends on several factors: the electron density, the flux at a given frequency and the shape of the ionizing continuum. Although the continuum flux at 0.1 Ryd illuminating 1 cm $^2$  of gas at the inner-radius of the coronal line region was fixed to be the same in all four models, the different ionizing continuum shapes result in a different number of ionizing photons and hence give rise to a different ionization parameter at the inner-radius.

For ease of visual comparison, the results for the various models presented in Figs. 3, 4, 5 and 6 are plotted against units of  $\text{Log } U$  for the non-thermal, unattenuated continuum model (Model NT) at the inner-radius of the coronal line region. The conversion from  $\text{Log } U$  for the other three models to that of Model NT was achieved by adding the difference in  $\text{Log } U$  between the other models and Model NT ( $\Delta \text{Log } U$ , which was calculated using the data given in Table 1). For example, for gas with an electron density of  $10^4$  cm $^{-3}$  the ionization parameter for Model NT is  $\text{Log } U = -1.06$ . However, for Model NTA the ionization parameter is  $\text{Log } U = -2.4$ , and hence  $\Delta \text{Log } U = 1.34$ . Although we present all results in units of  $\text{Log } U$  for Model NT, when we derive ‘best fit’ values of  $\text{Log } U$

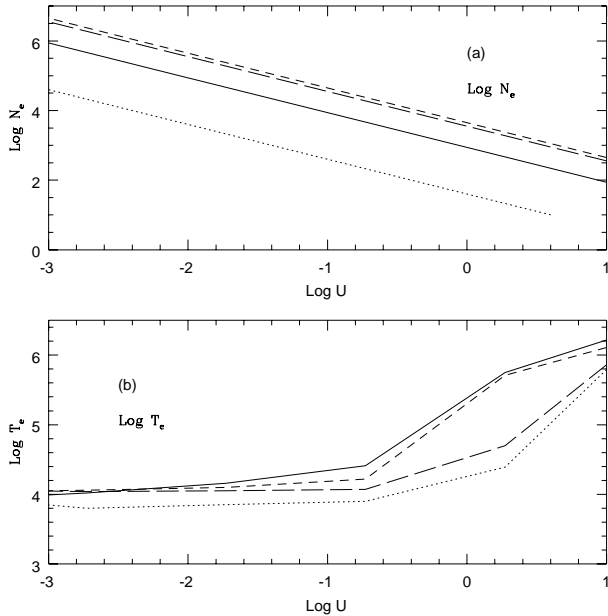


**Fig. 3.** The variation of  $\text{Log } N_e$  and  $\text{Log } T_e$  with  $\text{Log } U$ . The values of  $\text{Log } U$  correspond to those for Model NT (see text for details). The solid line is for Model NT, the small dashed line is for Model NTS, the dotted line is for Model NTA and the long dashed line is for Model NTSA.

we also give the ionization parameters corresponding to the specific model being considered calculated from the value of  $\Delta \text{Log } U$ .

The flux of ionizing photons,  $N_{ph}$  ( $\text{cm}^{-2} \text{s}^{-1}$ ), in each model together with  $\text{Log } U$  at the inner-radius of the coronal line region for an electron density  $N_e = 10^4 \text{ cm}^{-3}$  are presented in Table 1. The relation between electron density,  $N_e$ , and  $\text{Log } U$  (Model NT) derived from the model grids for the four different models are shown in Fig. 3(a). The number of ionizing photons is the same for all electron densities for the same model, but  $\text{Log } U$  varies according to changes in the electron density.

The derived average electron temperature,  $T_e$ , in the coronal line region is shown in Fig. 3(b). The variation of  $T_e$  with  $\text{Log } U$  in Models NT, NTS and NTSA is similar for  $\text{Log } U \leq -2$ . For Model NTA when  $\text{Log } U \leq -0.3$ ,  $T_e \leq 10^4 \text{ K}$ . The attenuated Models NTA and NTSA show smaller increases in temperature with increasing ionization parameter compared to Models NT and NTS.

### 3.1. The coronal lines

The calculated coronal line intensities are shown in Fig. 4 for each model with several different electron densities. In Fig. 4 the variation in the ionization parameter for each specific continuum reflects the different densities of the emitting gas. Clearly, the shape of the central continuum strongly affects the lines for all models. Including attenu-

ation (Models NTA and NTSA) shifts the maximum line emission to higher ionization parameter compared to that for the unattenuated continua (Models NT and NTS). This is due to the smaller ionization parameter for the attenuated continua, as discussed previously (see Table 1).

The calculated high-ionization coronal line ratios for each model are shown in Fig. 5, together with the observed ratios from Marconi et al. (1996) for NGC 1068, and from Oliva et al. (1994) for the Circinus galaxy. As noted, a higher ionization parameter is required to fit the high-ionization line strengths with the attenuated continua (Models NTA and NTSA) compared to the unattenuated continua (Models NT and NTS).

#### 3.1.1. NGC 1068

It can be seen from Fig. 5 that model line ratios close to those observed in NGC 1068 (solid horizontal lines) correspond to different ionization parameters. For example, the observed  $[\text{Fe XI}]/[\text{Fe X}]$  ratio corresponds to an ionization parameter  $\text{Log } U \approx -1$  for Model NT, whereas the  $[\text{Fe VII}]/[\text{Fe X}]$  ratio corresponds to  $\text{Log } U \approx -1.5$ . Similarly, a difference of  $\Delta \text{Log } U \approx 2$  is found between the  $[\text{Si IX}]/[\text{Si VIII}]$  and  $[\text{Fe XI}]/[\text{Fe X}]$  ratios for Model NT. The  $[\text{Si IX}]/[\text{Si VI}]$  and  $[\text{Fe VII}]/[\text{Fe X}]$  ratios correspond to a similar  $\text{Log } U$  for Model NTSA, whereas the  $[\text{Fe XI}]/[\text{Fe X}]$  and  $[\text{Si IX}]/[\text{Si VIII}]$  ratios correspond to very different ionization parameters.

Because the observed coronal line ratios in NGC 1068 are difficult to explain with a single ionizing continuum shape, we investigated whether they could be fitted using a mixture of gas illuminated by unattenuated and attenuated continua. Line ratios for such a mixture of gas components are shown in Fig. 6, where the value  $r = \text{NT}/\text{NTA}$  and  $r = \text{NTS}/\text{NTSA}$  denotes the relative contribution of line emission from the unattenuated and attenuated models. When  $r = 1$  the lines are emitted from the attenuated and unattenuated models in equal proportion. When  $r = 0.7$  the unattenuated and attenuated models contribute 41% and 59% respectively of the line emission. When  $r = 0.5$  the contributions are 33% and 66% respectively.

From Fig. 6, we find the best-fit solution for NGC 1068 for the 3 high-ionization coronal line ratios is with  $r = 0.7$  for Models NT (41%) and NTA (59%) and  $\text{Log } U = -1$ . From Fig. 3(a) this ionization parameter corresponds to  $N_e \approx 10^4 \text{ cm}^{-3}$ . This electron density is quite close to the  $N_e \geq 10^{4.5} \text{ cm}^{-3}$  derived by Axon et al. (1998) from the  $[\text{Ar IV}]\lambda\lambda 4710/4740$  line ratio. The difference in the electron density obtained by Axon et al. and the electron density estimated by our modelling could be due to the very different spatial resolutions of the IR/optical (Oliva et al. 1994; Moorwood et al. 1996) and HST spectra. Axon et al. obtained a spectrum with a slit projected along the jet and found dense blobs inside of the jet, whereas the

**Table 1.** The parameters of the models for  $N_e = 10^4 \text{ cm}^{-3}$ .

Models	NT	NTA	NTS	NTSA
Log $N_{ph}$	13.41	12.07	14.12	14.00
Log U	-1.06	-2.40	-0.35	-0.45

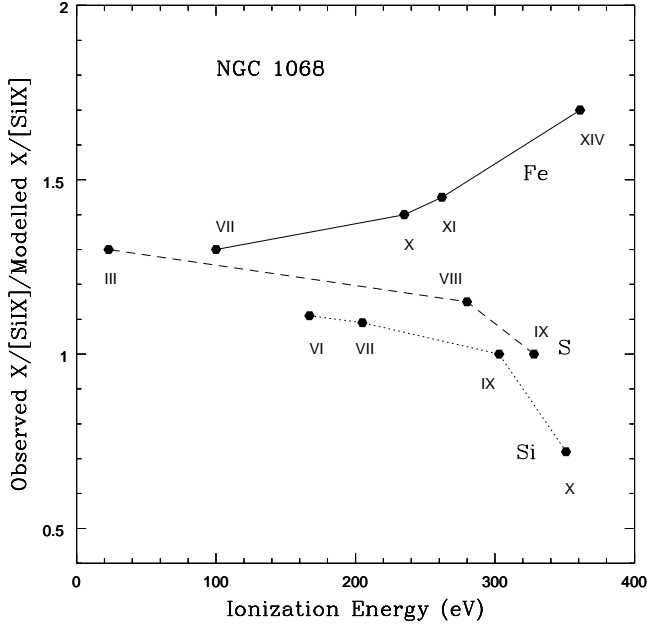


**Fig. 7.** Observed divided by modelled flux ratios in NGC 1068, for the NT+NTA model with  $r = 0.7$ . All ratios are expressed relative to  $[\text{Si IX}]3.935\mu\text{m}$ . The observed intensities of the lines  $[\text{Fe VII}]\lambda 6087$ ,  $[\text{Fe X}]\lambda 6375$ ,  $[\text{Fe XI}]\lambda 7892$ ,  $[\text{Fe XIV}]\lambda 5303$ ,  $[\text{Si VI}]\lambda 1.963(\mu\text{m})$ ,  $[\text{Si VII}]\lambda 2.483(\mu\text{m})$ ,  $[\text{Si IX}]\lambda 3.9346(\mu\text{m})$ ,  $[\text{S III}]\lambda 9052$ ,  $[\text{S VIII}]\lambda 9912$  and  $[\text{S IX}]\lambda 1.25235(\mu\text{m})$  are taken from Marconi et al. (1996). The observed intensity of the  $[\text{Si X}]\lambda 1.4305(\mu\text{m})$  line was taken from Thompson (1996).

ground-based IR/optical spectra average over the coronal line region.

The ratio of the observed to modelled (NT+NTA,  $r = 0.7$ ) line fluxes as a function of ionization energy for NGC 1068 are shown in Fig. 7. The model shows a reasonably good fit for the sulphur, silicon and iron coronal lines. We note that the ionization parameter,  $\text{Log U} = -1$  quoted above and obtained from the best-fit NTA+NT model, is in units of  $\text{Log U}$  for Model NT. Using the data in Table 1 (Section 3), the “true” ionization parameter for 41% Model NT + 59% Model NTA ( $r = 0.7$ ) is  $\text{Log U} \approx -1.4$ .

We did not find a reasonable solution for NGC 1068 using the non-thermal+stellar continua (the NTSA+NTS models) for the 3 line ratios shown in Fig. 6. The  $[\text{Fe VII}]/[\text{Fe X}]$  and  $[\text{Si IX}]/[\text{S VIII}]$  ratios do not strongly depend on the relative contribution of the attenuated and

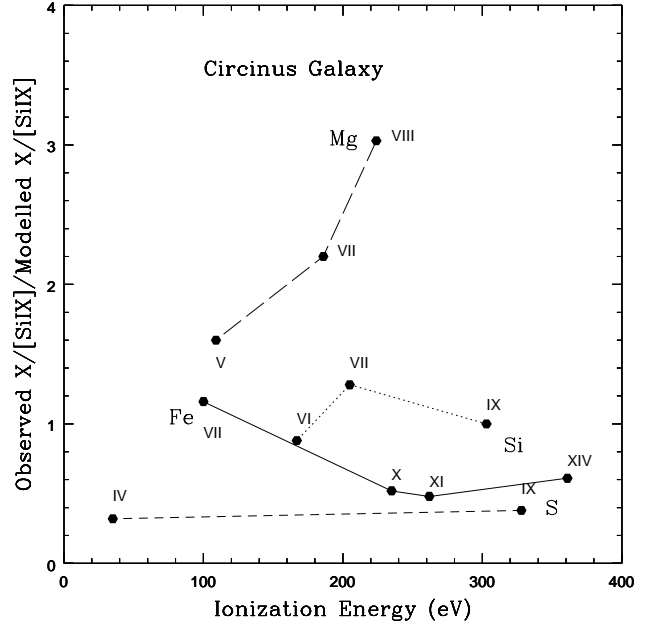


**Fig. 8.** Observed divided by modelled (Model NTA) flux ratios in the Circinus galaxy. All ratios are expressed relative to  $[\text{Si IX}]3.935\mu\text{m}$ . The intensities of the lines  $[\text{Fe VII}]\lambda 6087$ ,  $[\text{Fe X}]\lambda 6375$ ,  $[\text{Fe XI}]\lambda 7892$ ,  $[\text{Fe XIV}]\lambda 5303$ ,  $[\text{Si VI}]\lambda 1.963(\mu\text{m})$ ,  $[\text{Si VII}]\lambda 2.483(\mu\text{m})$ ,  $[\text{Si IX}]\lambda 3.9346(\mu\text{m})$ ,  $[\text{S IV}]\lambda 10.54(\mu\text{m})$   $[\text{S IX}]\lambda 1.25235(\mu\text{m})$  are taken from Oliva et al. (1994). The intensity of the lines  $[\text{S IV}]\lambda 10.54(\mu\text{m})$ ,  $[\text{Mg V}]\lambda 7.66(\mu\text{m})$ ,  $[\text{Mg VII}]\lambda 5.51(\mu\text{m})$  and  $[\text{Mg VIII}]\lambda 3.03(\mu\text{m})$  are taken from Moorwood et al. (1996).

unattenuated models, whereas the  $[\text{Si IX}]/[\text{Si VI}]$  ratio does depend strongly on their relative contribution. When  $r=1$  (equal contribution from attenuated and unattenuated models) the  $[\text{Si IX}]/[\text{Si VI}]$  ratio is shifted to lower ionization parameters for both the NTA+NT and NTSA+NTS continua. This is due to the decrease in the number of ionizing photons resulting from the higher relative contribution from regions which are illuminated by the attenuated continuum. The  $[\text{Si IX}]/[\text{Si VI}]$  ratio thus serves as an indicator of the relative contribution of gas illuminated by the attenuated and unattenuated continua.

### 3.1.2. The Circinus galaxy

Unlike NGC 1068, we were able to find a reasonable fit to the high-ionization coronal lines in the Circinus galaxy

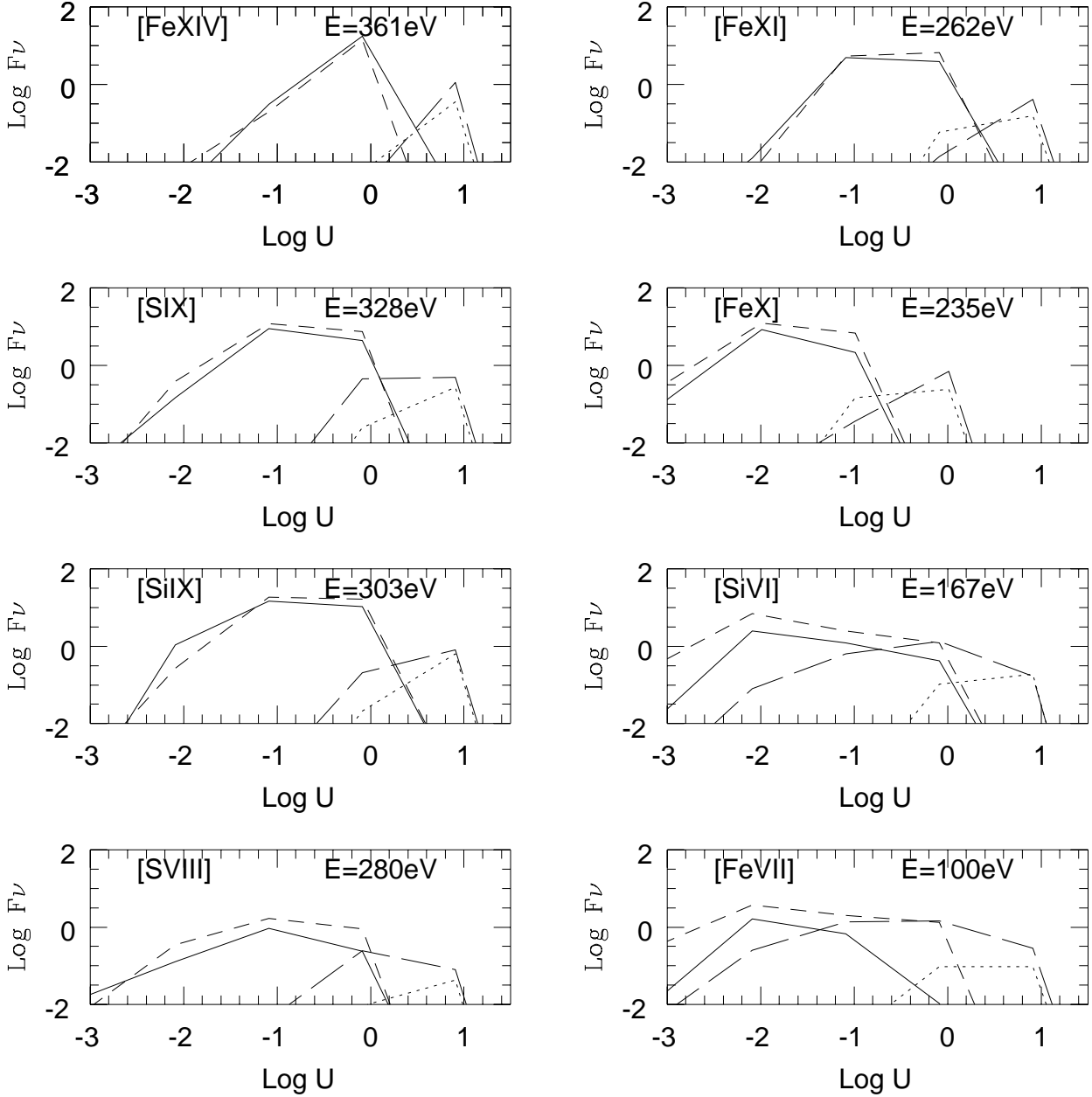


**Fig. 4.** The variation in line emission with ionization parameter for eight coronal lines, plotted in units of  $\text{erg cm}^{-2} \text{s}^{-1}$ . The numbers show the photon energies (in eV) needed to produce the ions of the coronal line parent species. The values of  $\text{Log } U$  correspond to those for Model NT (see text for details). The solid line shows the emission from  $1 \text{ cm}^2$  of the coronal line gas for Model NT (unattenuated, non-thermal continuum); the small dashed line shows the emission for Model NTS (the sum of unattenuated, non-thermal+stellar continua); the dotted line corresponds to the attenuated, non-thermal continuum (Model NTA); and the long dashed line corresponds to the attenuated, non-thermal+stellar continua (Model NTSA).

using a single model (i.e., a single continuum shape). From Fig. 5, the best-fit high-ionization coronal line ratios for the Circinus galaxy correspond to  $-0.8 \leq \text{Log } U \leq 0.8$  for the attenuated, non-thermal continuum (Model NTA),

with an average value  $\text{Log } U = 0$ . From Fig. 3(a) we estimate the electron density to be  $10^2 \leq \text{Log } N_e \leq 10^4 \text{ cm}^{-3}$ , with an average value,  $N_e = 10^3 \text{ cm}^{-3}$ . This electron density is similar to that derived by Moorwood et al. (1996)

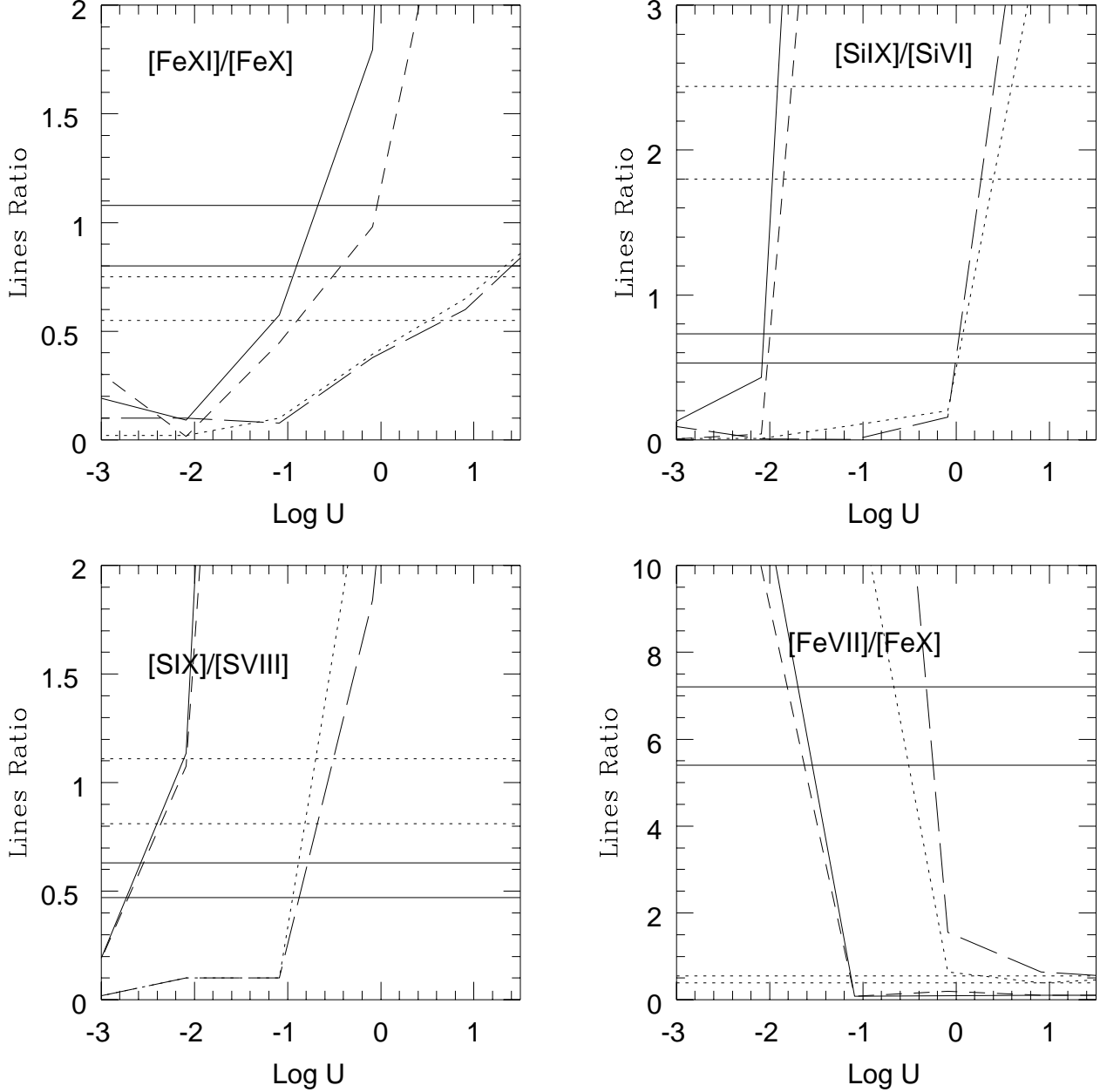


**Fig. 5.** The high-ionization coronal line ratios. The values of  $\text{Log } U$  correspond to those for Model NT (see text for details). The observed ratios in NGC 1068 are shown by the solid horizontal lines and the observed ratios in the Circinus galaxy are shown by the dashed horizontal lines. The photoionization model results are shown by the other lines, using the same notation as in Fig. 4.

from the density sensitive  $[\text{Ne } v]24.3(\mu\text{m})/14.3(\mu\text{m})$  ratio, which gives  $N_e = 5000 \text{ cm}^{-3}$ . We note that the ionization parameter,  $\text{Log } U = 0$  quoted above and obtained from the best fit NTA model, is in units of  $\text{Log } U$  for Model NT. From Table 1 (Section 3), the “true” ionization parameter for Model NTA equals  $\text{Log } U = -1.34$ .

The ratios of the observed to the modelled (Model NTA) line fluxes as a function of ionization energy for the different sulphur, silicon, iron and magnesium lines seen in the Circinus galaxy are presented in Fig. 8. The systematic deviation from unity (e.g. sulphur) might be due to peculiar abundances relative to solar. The different iron species from  $[\text{Fe VII}]$  to  $[\text{Fe XIV}]$  fit reasonably well using



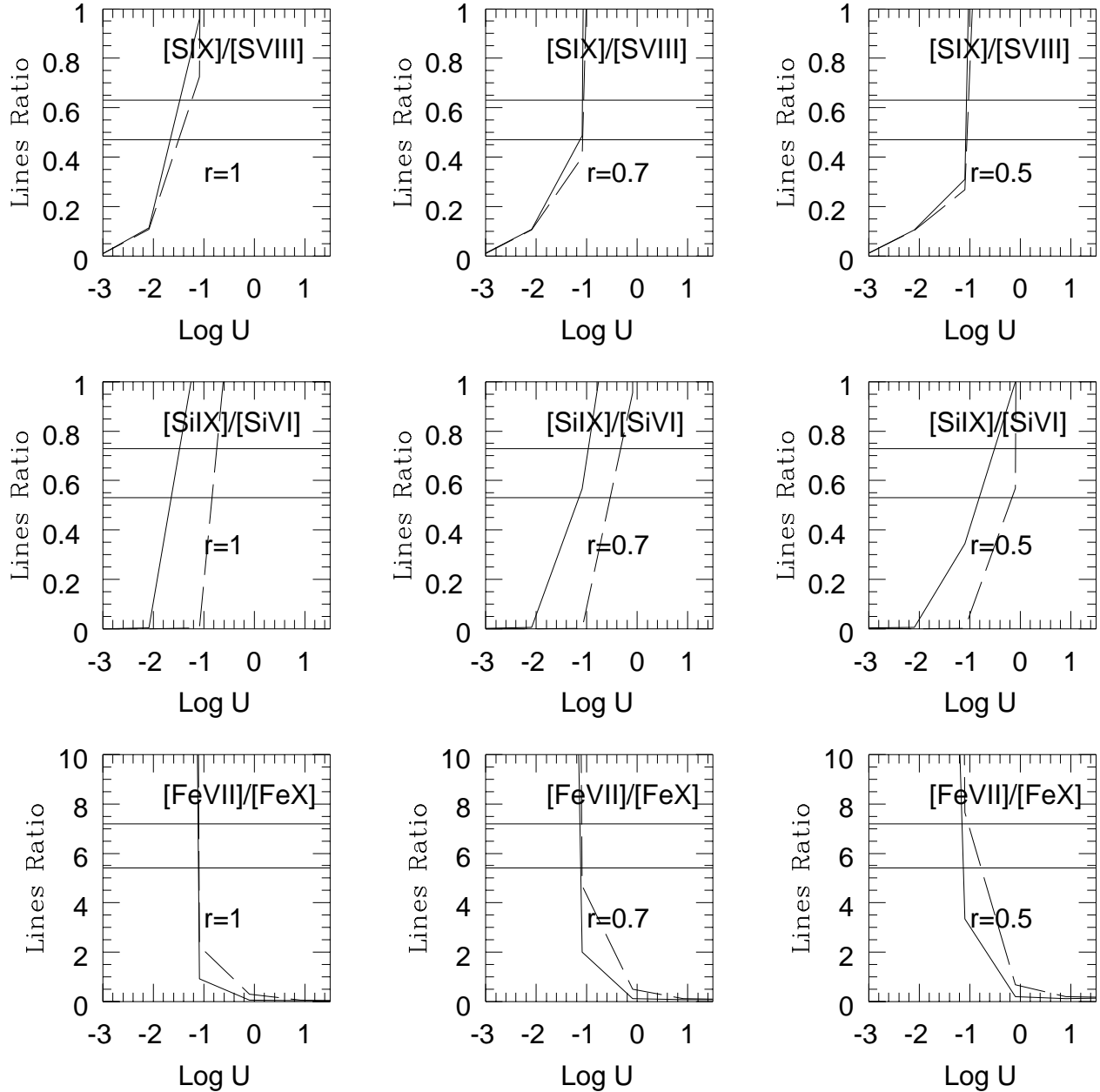


**Fig. 6.** The coronal line ratios for a combination of the attenuated and unattenuated models. The value  $r = NT/NTA$  or  $r = NTS/NTSA$  is the relative contribution of line emission from the unattenuated and attenuated models. The values of  $\text{Log } U$  correspond to those for Model NT (see text for details). When  $r = 1$  the lines are emitted from the attenuated and unattenuated models in equal proportion. When  $r = 0.7$  the relative contributions are 41% unattenuated and 59% attenuated and when  $r = 0.5$  the contributions are 33% unattenuated and 66% attenuated. The solid line corresponds to the pure non-thermal continua (NT and NTA) and the long dashed line corresponds to the sum of non-thermal and UV bump continua (NTS and NTSA).

the collision strengths adopted in CLOUDY. The details of the atomic data used are discussed in the CLOUDY manual (HAZY, Ferland 1996), the CLOUDY source code and Ferland et al. (1998)

#### 4. Discussion

The observed coronal line ratios indicate a somewhat lower excitation of the coronal line region in NGC 1068

than in Circinus, except for the  $[\text{Fe XI}]/[\text{Fe X}]$  ratio which is higher in NGC 1068. The  $[\text{Fe VII}]/[\text{Fe X}]$  ratio is 13 times higher and the  $[\text{Si IX}]/[\text{Si VI}]$  ratio 3.3 times lower in NGC 1068 than in Circinus. Based on these ratios, Marconi et al. (1996) suggested that the ionization parameter in NGC 1068 is lower and the ionizing continuum steeper than in Circinus. From our models, the different observed coronal line ratios in these two galaxies might be caused by different amounts of ionizing continuum attenuation. We derive similar ionization parameters in the coronal line region, but the derived electron densities differ by a factor of 10, being higher in NGC 1068. Thus, the number of ionizing photons in the coronal line region of the NGC 1068 is ten times higher than in the Circinus galaxy.

There are several possible sources of attenuation which could influence the observed coronal line emission. Binette et al. (1997) and others have considered the effect of attenuation produced within the coronal line clouds themselves (ionization stratification) and whether matter-bounded clouds could overlap along a line-of-sight to the nucleus producing continuum attenuation for ionization-bounded clouds at larger radii (shadowing within the coronal line region). While some ionization stratification seems likely, our models suggest that shadowing by gas in the coronal line region seems unlikely to be a major cause of attenuation in NGC 1068. Based on the observed luminosity of  $[\text{Si IX}]$ ,  $1.1 \times 10^{40}$  erg s $^{-1}$  (Marconi et al. 1996), and a nuclear continuum illumination-cone opening angle of  $\approx 80^\circ$  (Unger et al. 1992), the required coronal line gas covering factor is only  $\approx 7 \times 10^{-2}$ . For the Circinus galaxy, in contrast, assuming a cone opening angle also of  $\approx 80^\circ$ , the implied covering factor is  $\approx 1$ , consistent with that proposed by Oliva et al. (1994).

We propose that the different, relative attenuation of the continuum emission illuminating the coronal line regions in NGC 1068 and the Circinus galaxy might be due to a different geometrical distribution of the attenuating gas. This effect might be due to the nuclear radio-jet, which has a different intensity in these galaxies. Capetti et al. (1997) found a morphological connection between the optical NLR emission and the radio emission in the region near to the jet in NGC 1068. The NLR material along the radio jet is denser and has a higher ionization-state than the surrounding gas. Axon et al. (1998) also suggest that continuum anisotropy could be produced by azimuthal variations of the optical depth to ionizing photons.

To explain the required mixture of coronal line emission from gas illuminated by both attenuated and unattenuated continua in NGC 1068, we propose that the radio jet has swept out a channel through the coronal line region out into the NLR, pushing some gas aside as it went. Gas around the channel sees attenuated, non-thermal (nuclear) continuum, whereas coronal line gas within the channel sees unattenuated, non-thermal continuum. Thus, in this model, the coronal line emission in NGC 1068 comes from

regions both surrounding the channel around the jet axis and from within the channel itself. Most of the coronal line emission comes from close to the nucleus, within  $\approx 1''$ .

The Circinus galaxy has no very prominent radio jet near to the nucleus similar to that in NGC 1068, but it has peculiar, highly-polarized (up to 45%) radio lobes orthogonal to the galactic plane, which show a non-thermal spectrum, and features which may be evidence for outflow (Elmoultie et al. 1995). An  $[\text{O III}]$  ionization cone was also found by Marconi et al. (1994). However, the Fe II 1.64( $\mu\text{m}$ ) and H $_2$  2.12( $\mu\text{m}$ ) images show only weak extended H $_2$  emission in Circinus, suggesting that the jet is confined close to the nucleus (Davies et al. 1998). The observed blue-shift of the coronal lines ( $\approx 35$  km s $^{-1}$ ; Oliva et al. 1984) in Circinus is also much smaller than in NGC 1068 ( $\approx 300$  km s $^{-1}$ ; Marconi et al. 1996), consistent with the radio jet having a smaller effect in Circinus. Thus, it may be that the radio jet has been unable to clear a channel in the Circinus galaxy, and the coronal line emission comes only from gas illuminated by the attenuated, non-thermal (nuclear) continuum.

## 5. Conclusions

We have presented photoionization models for the coronal line spectrum in NGC 1068 and the Circinus galaxy. The line fluxes were calculated using four different ionizing continua: a non-thermal (nuclear) continuum (Model NT); the non-thermal continuum plus a UV bump (Model NTS); and attenuated versions of both these continua (Models NTA and NTSA). The attenuation of the continua was assumed to be caused by gas with column density  $10^{22}$  cm $^{-2}$  located within the inner-radius of the coronal line region.

For NGC 1068 the predicted  $[\text{Si IX}]/[\text{S VIII}]$ ,  $[\text{Si IX}]/[\text{Si VI}]$  and  $[\text{Fe VII}]/[\text{Fe X}]$  ratios agree best with the observations if about 40% of the line emission comes from gas illuminated by unattenuated, non-thermal continuum (Model NT) and about 60% from gas illuminated by attenuated, non-thermal continuum (Model NTA). The derived electron density and ionization parameter of the coronal line gas in NGC 1068 are  $N_e \approx 10^4$  cm $^{-3}$  and  $\text{Log } U = -1.4$ .

For the Circinus galaxy the predicted coronal line ratios fit best if all the gas is illuminated by attenuated, non-thermal continuum (Model NTA). The derived ionization parameter,  $\text{Log } U = -1.34$ , is very similar to that of NGC 1068. However, the derived electron density of the coronal line gas in Circinus,  $N_e = 10^3$  cm $^{-3}$ , is an order of magnitude smaller, implying a much higher photon flux compared to NGC 1068, explaining the different observed excitation state of the coronal line gas in the two galaxies.

We propose that the difference between the coronal line emission in these galaxies could be due to the different prominence of their respective radio jets. In this model, the stronger radio jet in NGC 1068 has swept out a chan-

nel as it passed through the coronal line region into the NLR, and therefore the radiation from the non-thermal continuum source suffers less attenuation along the jet axis. Coronal line gas within the channel sees unattenuated, non-thermal continuum, whereas coronal line gas in the region around the channel sees attenuated, non-thermal continuum. We observed the combined coronal line emission from both these regions. The less powerful radio jet in the Circinus galaxy has been unable to sweep out such a channel, and hence its coronal line region is illuminated only by attenuated, non-thermal continuum.

*Acknowledgements.* L.S.Nazarova wishes to thank the University of Leicester for their hospitality. We thank Gary Ferland for providing a copy of CLOUDY. The calculations were performed on SUN and DEC workstations provided by the PPARC Starlink project at Leicester. L.S.N would like to acknowledge support under The Royal Society grant. This work was also partly supported from INTAS 96-0328 and RBRF 96-02-17625 grants.

## References

- Alloin D., Pedlar A., Boksenberg A., Sargent W.L.W, 1983, ApJ, 275, 493
- Axon D.J., Marconi A., Capetti A., Macchetto F.D., Schreier E., Robinson A., 1998, ApJ, 496, L75
- Binette L., Wilson A.S., Storchi-Bergmann T., 1996, A&A, 312, 365
- Binette L., Wilson A.S., Raga A., Storchi-Bergmann T., 1997, A&A, 327, 909
- Bergeron J., Petijean P., Durret F., 1989, A&A, 213, 61
- Capetti A., Axon D.J., Macchetto F.D., 1997, ApJ, 487, 560
- Elmoultie M., Haynes R.F., Jones K.L., Ehle M., Beck R., Wielebinki R., 1995, MNRAS, 275, L53
- Evans N., Dopita M.A., 1986, ApJ, 310, L15
- Davies R.I., Forbes D.A., Ryder S., Ashley M.C.B., Burton M., Storey J.W.V., Allen L.E., Ward M.J., 1998, MNRAS, 293, 189
- Ferland G.J., 1996, Hazy, a brief introduction to CLOUDY 90, University of Kentucky Physics Department Internal Report
- Ferland, G.J., Korista, K.T., Verner, D.A., Ferguson, J.W., Kingdon, J.B., Verner, E.M., 1998, PASP, 110, 761
- Ferguson J.W., Korista K.T., Ferland G.J, 1997, ApJS, 110, 287
- Forbes D.A., Norris R.P., 1998, MNRAS, 300, 757
- Ghosh S.K., Bisht R.S., Iyengar K.V.K., Rengarajan S.N., Tandon S.N., Verna R.P., 1992, ApJ, 391, 111
- Greenfill L.J., Elingsen S.P., Norris R.P., Gough R.G., Sinclair M.W., Moran J.M., Mushotzky R., 1997, ApJ, 474, L103
- Korista K.T., Ferland G.J., 1989, ApJ, 343, 678
- Mathews W.G., Ferland G.J., 1987, ApJ, 323, 456
- Matt G., Fiore F., Perola G.C., Piro L., Fink H.H., Grandi P., Matsuoka M., Oliva E., Salvati M., 1996, MNRAS, 281, L69
- Marconi A., Moorwood A.F.M., Origlia L., Oliva E., 1994, Messenger, 78, 20
- Marconi A., Van der Werf P.P., Moorwood A.F.M., & Oliva E., 1996, A&A, 315, 335
- Moorwood A.F.M., Glass I.S., 1984, A&A, 135, 281
- Moorwood A.F.M., Oliva E., 1994, Infrared Phys. Tech., 35, 349
- Moorwood A.F.M., Lutz D., Oliva E., Marconi A., Netzer H., Genzel R., Sturm E., de Graauw Th., 1996, A&A, 315, L109
- Nazarova L.S., 1995, A&A, 299, 359
- Nazarova L.S., O'Brien P.T., Ward M.J., Gondhalekar P.M., 1998, A&A, 331, 471
- Oliva E., Moorwood A.F.M., 1990, ApJ, 348, L5
- Oliva E., Salvati M., Moorwood A.F.M, Marconi A., 1994, A&A 288, 457
- Oliva E., 1997, In 'Emission Lines in Active Galaxies: New Methods and Techniques', (eds. Peterson, B.M., Cheng, F.-Z., Wilson, A.S.), ASP Conference Series No.113, p.288
- Pier E.A., Antonucci R.R.J, Hurt T., Kriss G., Krolik J., 1994, ApJ, 428, 124
- Seyfert C.K., 1943, ApJ, 97, 28
- Telesco C.M., Harper D.A., 1980, ApJ, 235, 392
- Terlevich, R., Melnick, J., 1985, MNRAS, 213, 841
- Thatte N., Quirrenbach A., Genzel R., Maiolino R., Tecza M., 1997, ApJ, 490, 238
- Thompson R.I., 1996, ApJ 459, L61
- Tully R.B., 1988, Nearby Galaxies Catalog, Cambridge University Press
- Unger, S.W., Lewis, J.R., Pedlar, A., Axon, D.J., MNRAS, 258, 371
- Viegas-Aldrovandi S.M., Contini M., 1989, A&A, 215, 253